ARTICLES

Influence of Small Additions of Al_2O_3 on the Properties of the $Na_2O{\cdot}3SiO_2$ Glass

C. Leonelli,* G. Lusvardi, M. Montorsi, M. C. Menziani, L. Menabue, P. Mustarelli,† and L. Linati‡

Department of Chemistry, University of Modena and Reggio Emilia, Modena, Italy, Department of Chemical Physics and INFM, University of Pavia, Pavia, Italy, and Centro Grandi Strumenti, University of Pavia, Italy

Received: May 23, 2000; In Final Form: October 18, 2000

Changes in the structural properties of sodium alumino-silicate glasses of general formula $Na_2O{\cdot}xAl_2O_3{\cdot}(3-x)SiO_2$ were investigated as a function of Al_2O_3 concentration. The experimental evidences provided by density, elastic modulus, glass chemical resistance measures, ^{29}Si and ^{27}Al MAS NMR investigations were complemented by molecular dynamics simulations. While neither of the experimental techniques or computational investigation utilized in this study were able to furnish unequivocable responses for the rationalization of the measured properties of sodium alumino-silicate glasses, the synergistic application of experimental and computational techniques showed that the anomalies observed in bulk properties like density and elastic modulus find their origin in medium-range structural features.

Introduction

The silicate-based glasses have long been of interest in the past because of their broad applications; hence, structural models for their amorphous network have attracted numerous authors. It is well-known that there are few oxides which added in small percentages to soda-silicate or industrial soda-lime silicate glasses remarkably influence the glass properties by perturbing the short rang order (SRO) and the intermediate range order (IRO) of the original network. The SRO describes the environment of the atoms around the network former ions; in particular, the oxygens atoms can be classified as bridging oxygens (BO), non bridging oxygens (NBO) and three bridging oxygens (TBO). The IRO defines how the tetrahedra are linked to each other.

Alumina is probably the most studied in terms of modification induced in glass network, being classified among those oxides whose role depends on its concentration and the overall glass composition.

Sodium alumino-silicate glasses can be considered as modified silica glasses, where the modifications are made to reduce the melt viscosity and to ease formation of the glasses.[1] Alumina additions to sodium silicate glasses improve durability, and some of these glasses are characterized by interesting anomalies in physical properties such as refractive index, viscosity, density, and electrical conductivity, as a function of composition. For example, sodium alumino-silicate glasses of general formula $Na_2O{\cdot}xAl_2O_3{\cdot}(3-x)SiO_2$ show a maximum in the viscosity and a minimum in the activation energy for electrical conductivity at $R = Al/Na = 1.0$, and an anomalous property change, i.e., elastic modulus and microhardness, at about $R = 0.2-0.4$.[2]

Structural models derived by different experimental data have been proposed to explain these property changes. They are based upon changes in aluminum coordination,[3−7] introduction of triclusters,[8,9] and degree of network polymerization.[10−13]

The updated random network model derived from that proposed by Zachariasen, known as "modified random network" theory accounts for the described anomalies.[14] An interpretation at atomic level was given by molecular dynamics (MD) computer simulations, which were successful in explaining the minimum in the electrical conductivity activation energy for a ratio of $Al/Na = 1$.[15] In the computational procedure adopted in this paper, the Al ions were constrained to a 4-fold coordination; therefore, the initial hypothesis of a coordination change from 4-fold to 6-fold for the Al(III) ions at $R \geq 1$ was not tested. Moreover, the maximum in the Na diffusion activation energy and minimum in the Na site potential experimentally observed at $R = 0.2$ remained to be explained. An improvement on this topic was provided by Cormack et al.[16−18] that simulated the sodium alumino-silicate glass structures without structural constraints on the Al ions. They did not observe changes in the aluminum coordination and reproduced correctly the extrema at $R = 0.2$ and $R = 1$.

It was suggested that the Al(III) ions act as network formers all over the compositional range considered, the electrostatic neutrality being guaranteed by the formation of three bridging oxygen (TBO) species. The change in oxygen coordination from 2-fold to 3-fold was observed to be paralleled by a general change in the ring size distribution that stabilizes the alkali potential sites leading to a general decrease of the Na(I) ions diffusion mechanism. Therefore, they hypothesized that the observed anomalies in the experimental properties of these glasses might be a result in the shift of the percolated alkali diffusion channels from NBO-rich regions to AlO_4 rich regions.[16,19]

Detailed information on short-range structure of alumino-silicate glasses may be obtained by ^{27}Al and ^{29}Si solid-state

† Department of Chemical Physics.
‡ Centro Grandi Strumenti.
* Corresponding author. Dip. di Chimica, Facolta' di Ingegneria, Universita' degli Studi di Modena e Reggio Emilia, Via Campi 183, 41100 Modena. E-mail: leonelli@unimo.it. Tel.: +39 059 2056247. Fax: +39 059 373543.

10.1021/jp0018908 CCC: $20.00
Published on Web 01/12/2001

TABLE 1: Batch Compositions from the General Glass Formula $Na_2O \cdot xAl_2O_3(3-x)SiO_2$, where $R = Al_2O_3$ (mol %)/Na_2O (mol %)

	$x = 0.0$, $R = 0.0$		$x = 0.1$, $R = 0.1$		$x = 0.2$, $R = 0.2$		$x = 0.3$, $R = 0.3$		$x = 0.4$, $R = 0.4$	
oxide	mol %	wt %	mol %	wt %	mol %	wt %	mol %	wt %	mol %	wt %
Na_2O	25	25.58	25	25.15	25	24.73	25	24.32	25	23.93
SiO_2	75	74.42	72.5	70.71	70	67.13	67.5	63.7	65	60.32
Al_2O_3			2.5	4.14	5	8.14	7.5	12.01	10	15.75

NMR at the magic angle (MAS).[20] Early ^{29}Si NMR studies on sodium-modified glasses were reported by Maekawa et al.[21] They found that aluminum tends to be coordinated to SiO_4^{-4} tetrahedra of most polymerized states, in agreement with the Loewenstein's rule (the so-called Al−O−Al avoidance rule).[22] Aluminum tetrahedral coordination in $5Na_2O \cdot 5Al_2O_3 \cdot 90SiO_2$ glasses was reported by Prabakar et al.[23] More recently, ^{29}Si and ^{27}Al MAS NMR investigations were reported by Schmucker at al.,[24] who studied rapidly quenched glasses with $R \geq 1$, and by Lee et al.[25] who studied the substitution of Na^+ with Cu^+. The degree of aluminum avoidance in $SiO_2 \cdot NaAlO_2$ glasses was also investigated by Lee and Stebbins[26] who found a degree of avoidance greater than 0.93. However, to our knowledge, no ^{27}Al NMR investigations have been yet reported for $R < 1$, but for some spectra published by Jager et al.,[27] which we will discuss in the following.

In the present work the change in several chemical and physical properties as a function of alumina addition to a sodium silicate glass of composition very close to that of industrial float glass have been measured in order to obtain insight into the anomalous property behavior pointed out in the literature. Such compositions, $Na_2O \cdot xAl_2O_3 \cdot (3-x)SiO_2$ where $x = 0.0$, 0.1, 0.2, 0.3, and 0.4 mol %, had never been experimentally characterized before. The structural details obtained by molecular dynamics simulations are analyzed in terms of short and midrange structure as embodied in the coordination number of each species (CN), the distribution of nonbridging oxygens (NBO) over the Si tetrahedral sites (Q^n) and Al tetrahedral sites (q^n), and the ring size distribution (RSD). Comparison between NMR and computational information will help to understand the structure length scale at which the anomalies observed in the bulk properties (density, elastic modulus, and chemical resistance) take place.

Experimental Section

The batch $Na_2O \cdot xAl_2O_3 \cdot (3-x)SiO_2$ compositions of the examined glasses are given in Table 1: such compositions were chosen so that to have a variability of the R parameter between 0.0 and 0.4, respectively when $x = 0.0$, 0.1, 0.2, 0.3, and 0.4 mol % (because of system stoichiometry, x coincides with the Al/Na ratio R). Reagent grade raw materials, Na_2CO_3 (RPE, Carlo Erba), Al_2O_3 (Aldrich-Chemie), and SiO_2 (Sikron 300), were mixed in polyethylene bottle with alumina balls for 30 min at low speed to allow homogenization. Glasses were melt in Pt crucible at 1500 °C for 4 to 6 h, depending upon composition, then poured onto graphite mold to obtain $1 \times 1 \times 10$ cm^3 slabs. Annealing treatments were performed for all compositions at about 500 °C for 30 min. Further sample preparation operations were performed in water-free silicon oils to avoid hydration.

Density was determined by the Archimedes' principle in mercury at room temperature on different samples for each composition with an accuracy of 0.002 g/cm^3. Each value is an average of three measurements on two different samples from the same composition.

Dynamic elastic modulus of rectangular base prisms was measured accordingly to ASTM C-885 on more than one sample for each composition (GrindoSonic, Lemmens, Belgium). Experimental error is minor than 1%.

Leaching tests were run for a ratio of 10 cm^2 of glass surface per 100 cm^3 of buffer solution at pH = 5. Each sample in form of a glass slice $1 \times 1 \times 0.1$ cm^3 was immersed in the solution of the test bottle and kept suspended to avoid contact with the magnetic stirrer used to continuously mix the solution. Test temperatures were 0 and 40 °C. Withdrawals were made at 10, 20, and 30 min and 1, 2, 7, and 16 h for two different samples each measurement. After the leaching time indicated above the solutions were tested by ICP-AES for determining Na, Al, and Si contents. Data are reported as grams per unit of surface area to get comparable values.

Both ^{29}Si and ^{27}Al MAS NMR data were collected with a AMX400WB spectrometer (Bruker, Germany, $B_0 = 9.4$ T), at Larmor frequencies of 79.46 and 104.2 MHz, respectively. ^{29}Si spectra were acquired using a 7 mm probehead (Bruker) equipped with cylindrical zirconia rotors and a boron nitride stator. The samples were spun at 4 kHz and the data were averaged over 1000 acquisitions using a single-pulse sequence, with a 30° pulse of 3 μs and a recycle time of 30 s. The spectra were referenced to TMS.

^{27}Al spectra were acquired using a 4 mm probehead (Bruker) equipped with cylindrical zirconia rotors and a boron nitride stator. The samples were spun at 13.5 kHz and the data were averaged over 2000−4000 acquisitions using a single-pulse sequence, with a 15° pulse of 0.4 μs and a recycle time of 100 ms. This small flip angle was chosen in order to allow a semiquantitative estimate of the ^{27}Al ($I = 5/2$) central transition.[28] The spectra were referenced to $Al(H_2O)_6^{3+}$. Neither left shifts nor line broadenings were applied during the data processing. All the spectra were analyzed using the WIN NMR package (Bruker).

Computational Procedure. MD simulations were performed with the DL_POLY[29] program at the CICAIA (Centro Interdipartimentale Calcolo Automatico e Informatica Applicata) of Modena and Reggio E. University, using Cerius2 (MSI)[30] as a graphical interface.

All the compositions experimentally characterized in this work were simulated by using as input structure a simulation box constituted by 27 β-cristobalite unit cells. Fifty percent of the Al^{3+} ion stoichiometric amount was introduced by substituting Si^{4+} ions and the remaining amount was introduced randomly in interstitial sites together with Na(I) ions and extra oxygens. Periodic boundary conditions were applied to the simulation box. The short-range interactions between Si−O and Al−O were modeled by a four-range Buckingham.[29] Three-body screened Vessal potential[31] was applied to O−Si−O, but not to O−Al−O to avoid assumptions about the coordination number of Al−O polyhedra. A simple Buckingham potential codifies the alkali-O short-range interactions.

The initial structure was melted at 6000 K and then cooled to 3000 K, and again to 1500 K and finally to 298 K. At each temperature a 10.000 time steps relaxation was allowed, at a time step of 2 fs. During the first 3000 of this 10.000 time steps the velocity was scaled every time step. During the second 3000

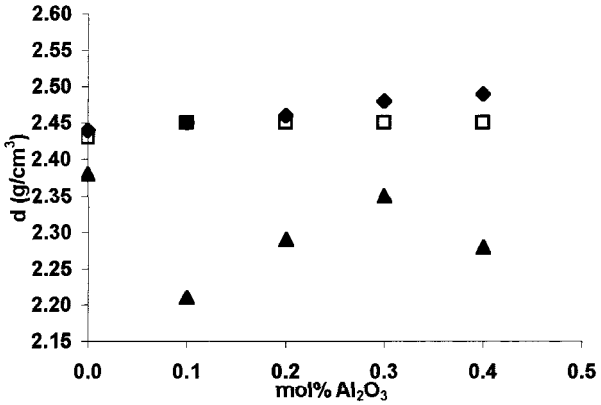

Figure 1. Density vs alumina content (◆, Appen and □ Huggins methods; ▲, experimental values).

time steps velocity scaling every 40 time steps was performed and, finally, during the last 4000 time steps no velocity scaling is applied. Constant volume simulations with Evans thermostat (NVT) were carried out at the higher temperatures, then the NVE ensemble was used. The starting volumes of the system were increased up to 5%, to account for the estimate thermal expansion coefficient, and then scaled in order to reproduce the experimental density at the final simulation temperature.

Data collection was performed every 10 time steps during the last 1500 time steps of the MD run.

Results and Discussion

Density. Because of the nature of glass as a "solution" of the various component oxides, ideas concerning the use of additivity factors for the calculation of the density ρ of glasses have been studied in great detail.[32] The experimental values of the understudied glasses have been compared to Huggins and Appen semiempirical methods (Figure 1).[33] The minimum in density recorded in the experimental data for $x = 0.1$ is not predicted by the mathematical approaches, being the experimental error on the third figure of each ρ value. Hence, the indication of a transition structure can be located at variation of the x value from 0.1 to 0.2, corresponding to $R = 0.1$ and 0.2, respectively.

As density does not depend only on the packing of atoms, but also to considerable degree on their mass, a comparison is possible only with glasses that contain oxides whose molar weights are similar (e.g., SiO_2, CaO, Na_2O). With glasses consisting of components with dissimilar molar weight, e.g., Al_2O_3 in this case, it is convenient to compare the glasses on the basis of unit molar volume V_1, related per gram atom of oxygen, expressed in cm^3 per gram atom of O^{-2}.[33] In a multicomponent glass, as it is the case, the unit volume V_1 is expressed as

$$V_1 = V_M/n_O = W_g/(\rho n_O) \quad (1)$$

where V_M is the molar volume of glass (cm^3/mol), ρ is the experimental density, W_g is the molar weight of glass (Σ molar fraction times the molecular weight of each single oxide), and n_O is the mean number of oxygen ions (Σ molar fraction times the number of oxygen per each oxide). As reported in Table 2, V_1 has the expected opposite behavior with respect to density with a maximum at $x = 0.1$. The reciprocal value of V_1 signifies the number of oxygen gram atoms per cm^3 of glass (O cm^{-3}) and can be directly correlated to some glass properties (T_g, η, E, and α) which also depend simultaneously on the density of cross-linking, DN.[33] With a multicomponent silicate glass containing alumina, the measure is provided by

TABLE 2: Volume Characteristic of the Investigated Glasses

composition x	W_g	n_O	V_1 (cm^3 gram atom O^{2-})	N_{Si}	N_{Al}	D_N
0	60.542	1.75	12.719	0.4286		1.336
0.1	61.6112	1.775	15.706	0.4045	0.0282	1.42
0.2	62.6365	1.8	15.196	0.3889	0.0556	1.499
0.3	63.6835	1.825	14.849	0.37	0.0822	1.577
0.4	64.7305	1.85	15.346	0.3514	0.1081	1.647

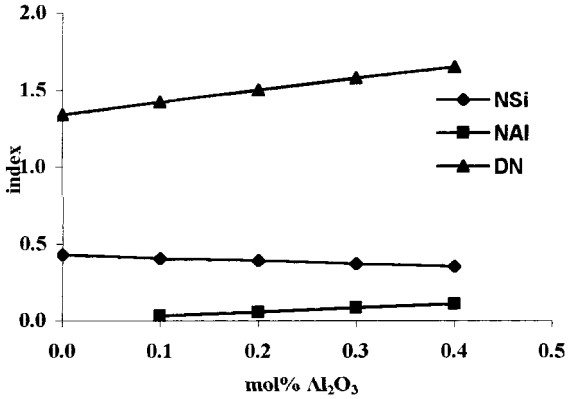

Figure 2. Cross-linking indices of N_{Si}, N_{Al}, and DN vs alumina content.

$$DN = 6 - [2/(N_{Si}+N_{Al})] \quad (2)$$

where $N_M = (m_{M,i}m_i)/(\Sigma n_{O,i}m_i)$, m_i being the molar percent, $m_{M,i}$ number of atoms of the electropositive element in the ith oxide molecule M_mO_n, and $n_{O,i}$ number of oxygen atoms in the same ith oxide. So, from the adopted expression, the density of cross-linking, DN is expressed by the number of excessive bridging oxygen per the central ion of the network-forming element, Si and Al for aluminosilicates. In the understudied glass composition the value of DN increase uniformly with alumina content (Figure 2), confirming what was observed for the semiempirical method of Huggins and Appen, where the mere additivity procedure accounts for the transition region.

It can be stated that the volume characteristics derived from classical method involving additivity of oxidic components do not allow to estimate the transition region which is showed when the correction with experimental data is possible, such as in V_1 and its reciprocal function.

Elastic Modulus. Elastic modulus is one of the properties affected by the degree of cross-linking of the glass network as well as by the type of bonds and by the bonding strength.[34] So it happens that modulus E is proportional to cation field strength (z/a^2) of the M−O bond, while covalent bonds tend to increase E value.

Ray[35] introduced the term "specific" modulus of elasticity E_s:

$$E_s = E/\rho \quad (3)$$

which was found to be proportional to the ratio:

$$\Sigma (m_i n_{O,i})/(m_i W_i) \quad (4)$$

where W_i is the molecular weight of the M_mO_n oxide.

The flexural elastic modulus presents two maxima, one at $x = 0.1$ and a second at $x = 0.4$, with a minimum at $x = 0.2$ (Figure 3). This behavior and the values obtained fits perfectly

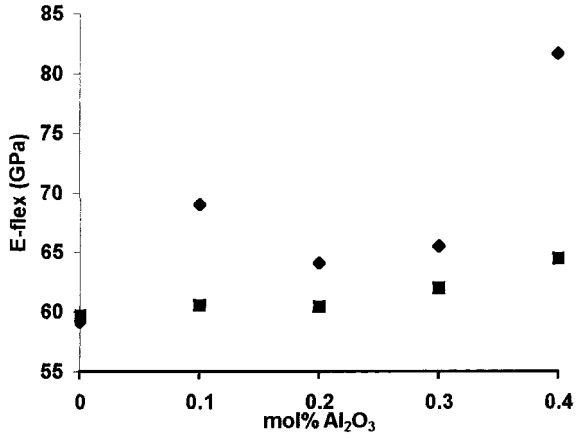

Figure 3. Flexural elastic modulus vs alumina content, (■, data from ref 36).

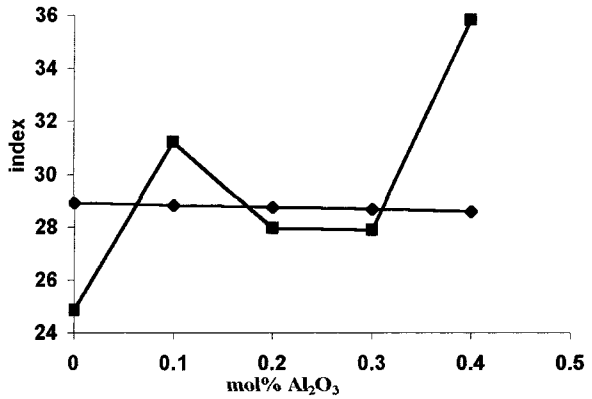

Figure 4. Indices for (■) E_s and (◆) ratio $\Sigma (m_i n_{O,i})/(m_i W_i)$ vs alumina content.

with those found for same glass composition by LaCourse and co-workers[36] who used the flexural resistance tests to determine the *E* value.

When E_s is reported in the same plot with the ratio (4) versus alumina content it appears that also for this property the discontinuity in the experimental behavior cannot be predicted by simply additive methods (Figure 4). E_s follows the E behavior, while ratio (4) is almost constant.

Chemical Properties. The glass chemical resistance has been measured as a function of time, from 10 min to 16 h, and temperature, $T = 0$ °C and $T = 40$ °C, to evaluate the diffusion of ions in the glass structure. Of the two different release mechanisms, sodium is more affected by leaching rather than by dissolution, as it is for aluminum and silicon. So the data for Na, quantities determined in the leaching solution, are 3 orders of magnitude higher than those for Al and Si and are presented separately (Figures 5 and 6). In the study of release as a function of time, Na atoms present in solution shows a decrease as Al_2O_3 is added to the glass, reaching a minimum between $x = 0.1$ and $x = 0.2$, and are time independent. Si and Al remain practically constant at few ppb with no influence of alumina addition or time.

As temperature increases, 40 °C, it can be noticed a great influence on the Na release after 16 h for $x = 0$, while the effect on the two other compositions is less evident. At 40 °C the minimum for $x = 0.2$ is no more evident for Na plot (Figure 7).

NMR Investigations. *(a) ^{29}Si spectra.* Figure 8 shows the ^{29}Si MAS NMR spectra of some selected samples. The Gaussian deconvolution scheme is also reported. The best-fitting parameters are reported in Table 3, together with other quantities which will be discussed in the following. Sample $x = 0.0$ shows two peaks (A) at −90.9 and (B) −103.8 ppm, which are attributed to Q^3 and Q^4 units, respectively. The ratio Q^4/Q^3 is 0.55, in good agreement with the previous one (∼0.5) reported in the literature,[37] and with the value theoretically given by the relationship for Q^3 formation in $xNa_2O:(1-x)SiO_2$ glasses for $x \leq 0.33$.

$$Q^3 = 2x/(1-x) \tag{5}$$

The addition of Al_2O_3 causes a progressive merge of the two features observed for $x = 0.0$. This effect was already reported in the literature.[21] However, a spectral decomposition is still possible, and the relative values are reported in Table 3.

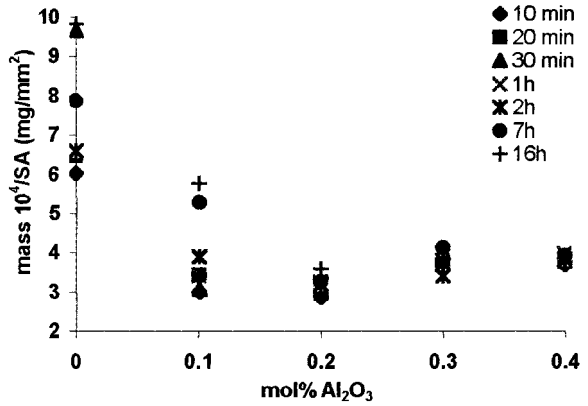

Figure 5. Released quantities of sodium at $T = 0$ °C at the times indicated.

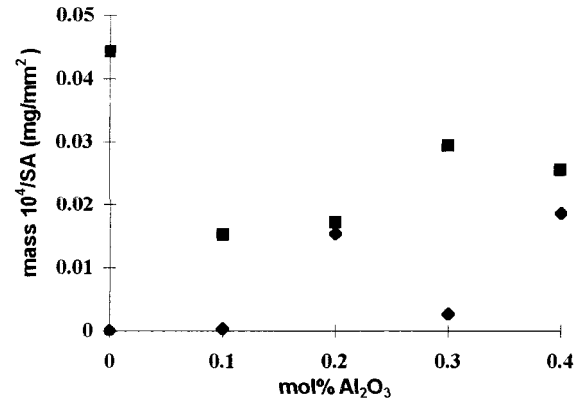

Figure 6. Released quantities of (◆) aluminum and (■) silicium at T=0 °C after 10 min.

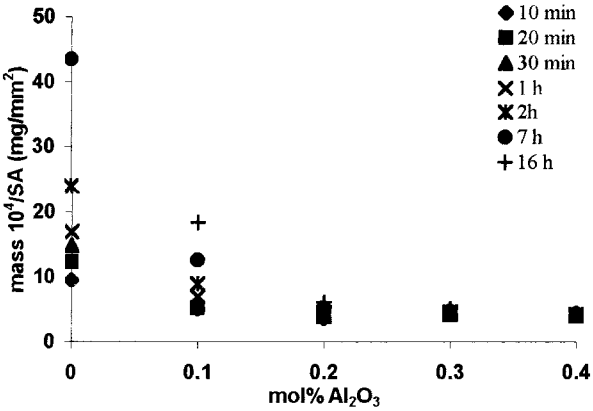

Figure 7. Released quantities of sodium at $T = 40$ °C at the times indicated.

TABLE 3: Best-Fitting Parameters of the ^{29}Si MAS NMR Spectra

	peak A			peak B			estimated areas[a]	
composition x	chemical shift (ppm)	fwhh (Hz)	area (%)	chemical shift (ppm)	fwhh (%)	area (%)	peak A	peak B
0.0	−90.9	903	0.655	−103.8	900	0.345	0.67	0.33
0.1	−90.4	934	0.63	−101.4	979	0.37	0.60	0.40
0.2	−88.3	957	0.60	−96.6	1215	0.40	0.54	0.46
0.3	−86.6	911	0.51	−94.8	1305	0.49	0.48	0.52
0.4	−85.4	896	0.45	−93.4	1102	0.55	0.41	0.59

[a] The areas are estimated on the basis on the model described in the text.

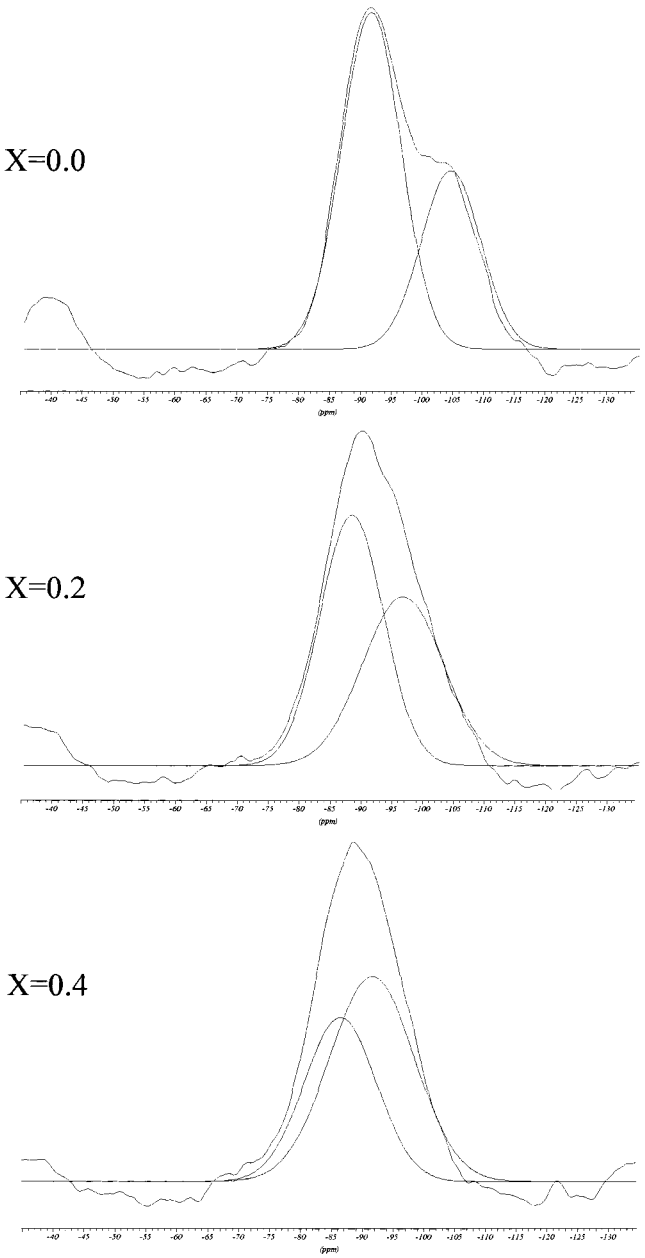

Figure 8. ^{29}Si MAS NMR spectra of samples $x = 0.0$, 0.2, and 0.4, together with their deconvolution schemes.

As already recalled, the addition of small quantities of Al_2O_3 to silicate glasses determines conversion $Q^3 \rightarrow Q^4$ and formation of Q^n(mAl) units.[20] In particular, each molecule of Al_2O_3 promotes two $Q^3 \rightarrow Q^4$ conversions. Moreover, (i) Al is preferably substituted in the most polymerized Q^n units and (ii) nearly all Al is tetrahedrally bound in the silicate network and follows the Loewenstein's rule.[38]

The expected chemical shifts of Q^n(mAl) can be obtained in terms of a simple empirical method proposed by Janes and Oldfield,[39] which is based on the electronegativities of the ligands to the silicon atoms. These values are reported in Table 4 together with some experimental data from the literature, while the chemical shifts we have obtained in the present work for Q^4(0Al) and Q^3(0Al) are shown in Table 3. We observe that the experimental values are systematically shifted several ppm downfield with respect to the estimated ones.

TABLE 4: Chemical Shifts of Some Q^n Units

Q^n-type unit	chemical shift (ppm) (Janes and Oldfield[39])	chemical shift (ppm) experimental data
Q^4 (0Al)	−107.4	−103 [ref 37]
Q^4 (1Al)	−101.6	
Q^4 (2Al)	−96.0	−93.4 [ref 40]
Q^4 (3Al)	−90.0	−88.7 [ref 40]
Q^3 (0Al)	−94.5	−88.5 [ref 41]
Q^3 (1Al)	−88.6	−78.9 [ref 40]
Q^3 (2Al)	−82.8	−74.0 [ref 40]
Q^2 (0Al)	−81.5	−76 [ref 42]

TABLE 5: Statistical Occurrences $P_{n,m}$ of Q^4 (mAl) Units in Aluminosilicate Glasses Computed According to Ref 43 (The MD Distribution is Reported in Parentheses)

composition, x	Q^4(0Al)	Q^4(1Al)	Q^4(2Al)
0.1	0.87	0.13	0.006
	(0.84)	(0.15)	(0.01)
0.2	0.75	0.23	0.02
	(0.71)	(0.27)	(0.02)
0.3	0.63	0.31	0.06
	(0.61)	(0.32)	(0.07)
0.4	0.53	0.37	0.1
	(0.55)	(0.40)	(0.05)

For the general case of a random Si, Al distribution which obeys to the Loewenstein's rule, the probability $P_{n,m}$, of the occurrence of the various Q^n(mAl) configurations can be calculated[43] by the binomial distribution

$$P_{n,m} = \frac{n!}{m!(n-m)!} p^m (1-p)^{n-m} \qquad (6)$$

where p is the ratio Al/Si. The probabilities of interest are reported in Table 5 for the different glasses compositions. We stress here that the values obtained by the binomial distribution are in good agreement with the MD results reported in parentheses in the same Table.

On the basis of the expected Q^n(mAl) chemical shifts and occurrences, reported respectively in Tables 4 and 5, we may suggest that our experimental peak B accounts for the progressive formation of Q^4(mAl) units ($m = 1, 2$) when Al_2O_3 is added to the sodium trisilicate glass. This explains the shift downfield for increasing x, and is also in agreement with the behavior of the peak width (full width at half-height (fwhh)), which is related to the level of disorder of the glass. Peak A, from its hand, accounts for the residual Q^3 units: fwhh remains roughly constant, and the average chemical shift is still in agreement with that reported in the literature (see Table 4). The relative intensities for peaks A and B expected from this simple model

TABLE 6: Best-Fitting Parameters of the ^{27}Al NMR Spectra

	peak A			peak B			peak C		
composition *x*	chemical shift (ppm)	fwhh (Hz)	area (%)	chemical shift (ppm)	fwhh (Hz)	area (%)	chemical shift (ppm)	fwhh (Hz)	area (%)
0.1	58	1145	46	50	1803	47	33	2243	7
0.2	58	1190	51	49	1648	41	32	1359	8
0.3	58	1279	60	48	1520	33	31	1325	7
0.4	57	1412	71	45	1451	24	32	1418	5

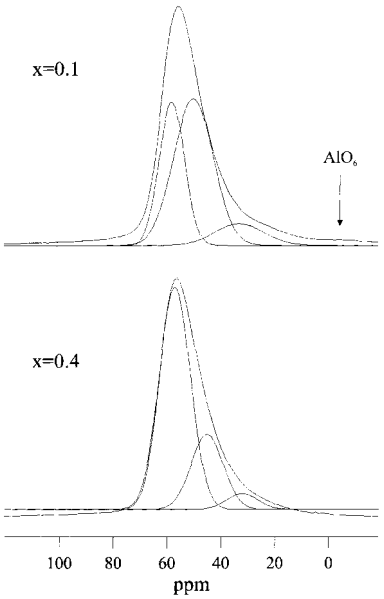

Figure 9. ^{27}Al MAS NMR spectra of the samples $x = 0.1$ and $x = 0.4$. The three peaks used in the best-fitting procedure are also shown.

can be obtained by using eqs 5 and 6, and are reported in Table 3. The agreement with experiment is good.

(b) ^{27}Al Spectra. Figure 9 shows the ^{27}Al MAS NMR spectra of the samples $x = 0.1$ and $x = 0.4$ together with their tentative deconvolution schemes (see following). The peak at ~50 ppm is given by aluminum in tetrahedral coordination, whereas the small feature at ~0 ppm which is observed only in the spectrum of $x = 0.1$ (scoring ~0.5% of the total) is due to Al nuclei in octahedral coordination.[20] The NMR spectra of the samples $x = 0.2$ and $x = 0.3$ are qualitatively similar to that of $x = 0.4$. At a first sight, we can conclude that the addition of Al_2O_3 does not change notably the aluminum coordination shell, at least in the range we explored, which is in agreement with the classical structural model.[20]

Jager et al.[27] recently proposed a tentative Lorentzian−Gaussian deconvolution of the ^{27}Al spectra of two sodium alumino-silicate glasses with composition similar to those we are examining. Thanks to a careful analysis of peak positions and widths vs the glass composition, the authors claimed to be able to extract information on the intermediate range order (IRO) and namely on the connectivity of the aluminum-centered structural units $Al(OSi)_n(O^-)_{4-n}$. Although we are well aware of the snares hidden in the nonlinear best fitting of such featureless curves, and also that the second-order electric quadrupolar effects cannot be fully rule out in our relatively high magnetic field (9.4 T), we will equally try to correlate our NMR information with the IRO results of molecular dynamics.

On the basis of the deconvolution scheme reported in Figure 9, three peaks are hypothesized at ~58 ppm (A), ~48 ppm (B), and ~33 ppm (C), respectively. Table 6 reports the nonlinear best fitting parameters for all the samples we examined. The RMS deviation of the fits is less than 5% in all cases. It can be noted that the intensity of peak A increases with *x* at the expenses of peak B, whereas the area of peak C is only marginally affected by Al_2O_3 content. The peak positions remain substantially unaffected, but for peak B that is slightly shifted upfield with increasing Al_2O_3. Concerning the peak widths, we observe that the full width at half-height (fwhh**)** of A increases with *x*, whereas that of B decreases. The width of C, finally, displays a large decrease (~40%) from $x = 0.1$ to $x = 0.2$, after that it remains nearly constant.

Following the discussion reported in ref 27, we can assign peak B to the AlO_4 tetrahedra connected with four SiO_4 units where all the oxygens are bridging (BO). These groups may be called $q^4(4Q^4)$, where the low-case q refers to aluminum, and Q^n indicates the silicon coordination. Peak A is assigned to aluminum in a less symmetric environment, for example to a unit $Al(OSi)_3(O^-\cdots Na^+)$. The chemical shifts of peaks A and B fall well in the 55−80 ppm range allowed for AlO_4 tetrahedra, if we recall that the center-of mass of the $^1/_2 \rightarrow -^1/_2$ central transition is affected by the second-order quadrupolar shift σ_{qs}. A rough estimate of the quadrupolar shift can be obtained from the relation $\sigma_{qs} = 0.85\Delta\nu_{1/2}$,[44] where $\Delta\nu_{1/2}$ is the fwhh value, which in our case give a value of about 15 ppm in the downfield direction. The feature at ~32 ppm should be attributed to distorted triclustered $(Si,Al)O_4$ tetrahedra, as suggested by Schmucker et al.,[24] rather than to pentacoordinated aluminum,[45] which is revealed to be unlike also by the MD results (see Table 8).

Our findings are in agreement with the structural model proposed by Galant,[46] that for $R < 1$ the Al^{3+} ions tend to form AlO_4 tetrahedra accompanied by Na^+ as charge compensators. This model accounts for the intensity increase of peak A with *R*, and the corresponding decrease of B, in qualitative agreement with the Al−NBO behavior as determined by MD (see Table 8). We recall here again that quantitative analysis of ^{27}Al NMR spectra is not simple because of quadrupolar interaction.[20] The width increase of peak A reflects the increasing structural disorder caused by the interstitial Na^+ ions.

Molecular Dynamics Simulations. Besides the compositions experimentally characterized in this paper we add, in the analysis of the molecular dynamics simulations, the results obtained in an our previous study[18] for a ratio $R = 2$ (which coincides with composition $x = 2$) in order to clarify the general trends of the structural modifications observed and facilitate the comparison with previously reported mechanistic conclusions.[16]

Perturbations in the SRO as a result of alumina additions are analyzed in Tables 7 and 8.

The percentage contribution to Al, Si, Na, and O coordination is listed in Table 7.

It is interesting to note that, notwithstanding the computational procedure chosen in this work deliberately avoids any assumption on the coordination preferences of the Al ions (see computational section) a 4-fold coordination over the entire compositional range can be observed, in agreement with the NMR results. The only significant amounts of Al defects are

TABLE 7: Percentage Contribution to the Al, Si, O, and Na Coordinations as a Function of Alumina Addition in the Glass

R =	CN				R =	CN					
Al/Na	3	4	5	6	Al/Na	1	2	3	4	5	6
Al					O						
					0.0	19.7	79.6	0.7	0.0	0.0	0.0
0.1	0.0	100	0.0	0.0	0.1	21.2	78.2	0.6	0.0	0.0	0.0
0.2	0.4	96.9	2.7	0.0	0.2	18.0	81.4	0.6	0.0	0.0	0.0
0.3	0.4	99.1	0.5	0.0	0.3	15.8	83.6	0.7	0.0	0.0	0.0
0.4	4.9	95.1	0.0	0.0	0.4	13.5	86.1	0.3	0.0	0.0	0.0
2.0	3.8	96.0	0.2	0.0	2.0	0.8	78.0	21.2	0.0	0.0	0.0
Si					Na						
0.0	0.7	79.2	17.4	2.8	0.0	0.4	9.1	37.6	34.7	14.7	3.1
0.1	1.3	85.7	12.8	0.2	0.1	2.1	16.1	42.8	25.9	10.2	1.6
0.2	2.1	84.1	13.1	0.7	0.2	1.1	17.1	41.9	28.3	10.3	1.2
0.3	3.0	84.0	12.5	0.5	0.3	1.7	14.6	35.9	33.8	11.4	2.4
0.4	1.1	88.4	9.8	0.6	0.4	2.1	18.9	44.1	27.6	6.9	0.5
2.0	4.3	93.0	2.9	0.0	2.0	2.3	14.9	29.4	31.9	16.5	4.6

TABLE 8: Contributions of BO, NBO, and TBO to the Fourfold Coordination of Si and Al Coordination Number

R = Al/Na	Si−BO	Si−NBO	Si−TBO	Al−BO	Al−NBO	Al−TBO
0.000	83.85	15.11	1.04			
0.100	83.65	16.34		99.82		0.17
0.200	83.30	14.39		93.13	2.32	4.54
0.300	85.43	13.67	0.90	96.30	4.03	1.34
0.400	88.71	10.73	0.56	96.06	3.69	0.25
2.000	85.90	2.06	11.95	67.25	0.00	32.75

observed for $R = 0.2$, 0.4, and 2 and are due to 5-fold and 3-fold Al sites, respectively.

The percentage of Si defects, with respect to coordination four, decreases as a function of Al addition, and it can be noted that for $R = 2$ the concentration of 3-fold Si defects becomes slightly greater than the concentration of high coordinated Si species.

Defects in Si coordination might be ascribed to the constraints imposed by constant volume simulations which put some restrictions on the relaxation processes the simulate systems will undergo. In fact, notwithstanding the computational procedure adopted allowed an increasing in the size of the box at high temperature to account for the estimated thermal expansion coefficient, the simulate glasses seem to be characterized by a high internal pressure. Five-fold Si sites are indeed experimentally observed in high pressured and rapidly quenched alkali glasses.[47]

Moreover, the figures show that the probability of the oxygen to be coordinated to a single silicon or aluminum atom diminished as R increase, while the concentration of triclusters rises up to 20% for glasses with $R = 2.0$. Finally, each sodium ion has a probability greater than 10% of being surrounded by two to five species, most likely three or four. This reflects the disordered nature of the Na site structure, coherently with its network-modifying role in the glass.

Interesting modifications induced by alumina addition to sodium silicate to the oxygen ion environment around the network former ions can be detected by analyzing the NBO, BO and TBO species distribution as a function of the glass composition.

Table 8 shows the contributions of BO, NBO and TBO to the 4-fold coordination of Si and Al. It is clear that the NBO contribution to the Si coordination number decreases with an increase of the R value although it is always greater that the NBO contribution to the Al coordination number, all over the compositional range under study. The decreasing of the NBO contribution to the Si ion coordination number is paralleled by an increase of the contribution of the TBO species.

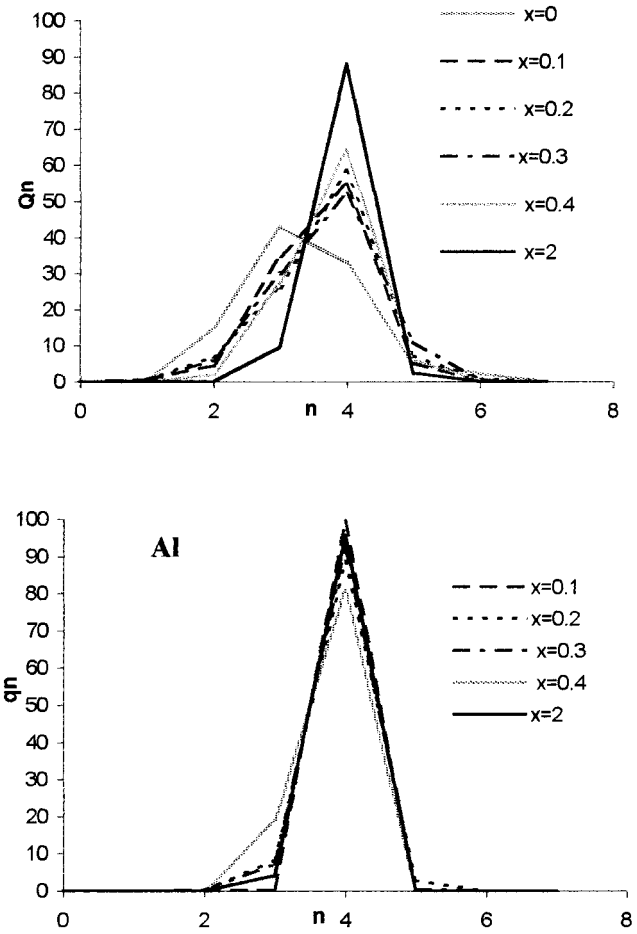

Figure 10. Q^n species distribution for the Si and the Al ions.

The Al ions are mainly coordinated by BO species, although, also in this case, the percentage decreases with an increasing of the R value. It is worth noting the anomalous values obtained for $R = 0.2$, where a consistent percentage of Al-TBO species is detected. A rough relationship between the Al-TBO trend and the behavior observed for the flexural elastic modulus (Figure 3) can be attempted.

The analysis of the Si tetrahedral sites (Q^n) and Al tetrahedral sites (q^n) distribution can be helpful for obtaining a picture of the IRO of the glass structure and in particular it allows a deeper understanding of the glass network complexity. This index is defined as the number of bridging oxygens surrounding a network former ion.

Overall the concentration of the Q^n and q^n species determined by MD simulations as a function of alumina addition (Figure 10) comapares reasonably with the experimental results.

However, the MD simulation for the sodium silicate glass ($x = 0$) shows a more equal percentage of Q^3 and Q^4 species with respect to the NMR results and a small percentage of Q^2 species not observed in the NMR spectra. Although these findings are in perfect agreement with previous molecular simulations studies,[48] it has to be recalled that discrepancies with the experimental results might be due to inappropriate simulation quench rates since the distribution of tetrahedral types is quite strongly temperature-dependent.[49]

No remarkable changes in q^n species as a function of R are noted for Al, a part for $R = 0.4$ which shows a 18% of q^3, in

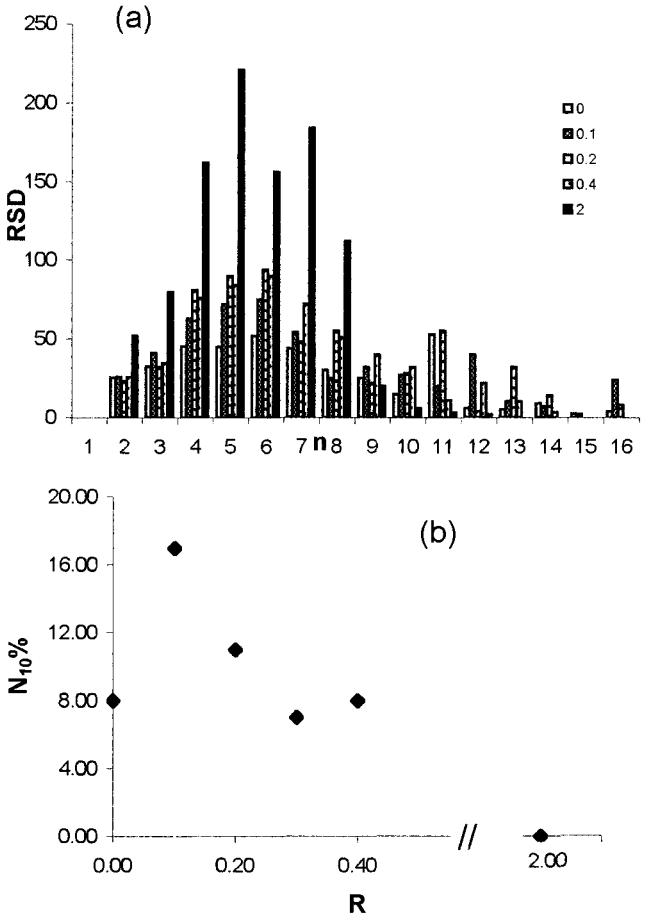

Figure 11. (a) Ring size distribution (RSD), (b) and normalized fraction of rings with more than 10 members for selected glass compositions.

agreement with the increase in peak A intensity as a function of R observed in the NMR deconvolution spectra. Moreover, consistently with the trend observed in Figure 2 for the DN empirical descriptor, an overall increase of the $q^n + Q^n$ seems to be due to significant progressive reduction of Q^3 sites for the Si ions, as a function of R. Since the presence of lower species types suggests the presence of sodium clustering in the network, the results clearly indicate that structural changes are induced on the Na ions distribution by the addition of alumina, as also underlined by the NMR results.

The IRO of the glassy structure is also investigated by analyzing the ring size distribution (RSD) reported in Figure 11 for selected compositions. The sodium silicate ($R = 0$) shows an almost uniform distribution of medium to large rings (up to 11 members). The large rings can be correlated to the high concentration of NBO species which prevent ring closure and ensure the presence of large channels for alkali migration in the network, making the glass nondurable and highly conductive, as pointed out by the chemical resistance experiments at 40 °C (Figure 7). The distribution of rings for $R = 0.1-0.4$ shows a maximum for six-members rings, moreover these glasses still present the ability of forming a sensible amount of rings at 10 or more members. In particular, an irregular distribution of large rings (up to 16) is found for $R = 0.1-0.3$, while for $R = 2$ a complete absence of big rings can be noted. Interestingly, $R = 0.4$ seems to be the limit composition at which the average ring size decrease started. Interestingly, the normalized fraction of rings with more than 10 members (Figure 11) shows an evident anomaly at $x = 0.1$, which is likely at the base of the anomalies observed in bulk properties like density, elastic modulus, and chemical resistance.

Conclusions

While neither of the experimental techniques or computational investigations utilized in this study were able to furnish unequivocable responses for the rationalization of the measured properties of sodium alumino-silicate glasses, the synergistic application of experimental and computational techniques gets valuable insights into the structural features responsible for their macroscopic behavior.

In particular, (a) the hypothesis that the Al ions enter in the network in a 4-fold coordination is substantiated, and (b) the experimental and theoretical q^n and Q^n distribution obtained by the NMR spectra and the analysis of the MD structure furnish a similar picture of the local order of the network structure as a function of the introduction of small amounts of Al. (c) The anomalies observed in density, elastic modulus and chemical resistance find their origin at intermediate range order, and can be correlated to the formation of triclusters and to the modification in the ring size distribution. This can hardly be monitored by solid-state NMR, which at best probes the next-neighboring structures, but falls well in the domain of MD calculations.

Finally, the results support a recently proposed model[16] for the interpretation of observed anomalies in the Na diffusion activation energy at $R = 0.2-0.4$, and at $R \geq 1$. In fact, on the initial addition Al perturbs the silica rich regions of the structure, substitutes the network forming silicon and creates AlO4 tetrahedra with four bridging oxygens, the excess of charges being balanced by moving Na ions from the alkali-rich network to the Al-silicate regions. Up to an Al/Na ratio of $R = 0.2$ the alkali-rich region remains continuous, but the concentration of alkali in these regions decreases and the size of the Si−O−Al islets increases, as it is observed by a visual inspection of the simulated glasses. In the range of concentrations $R = 0.2-0.4$ the continuous alkali-rich regions become increasingly disrupted, with formation of a continuous aluminosilicate network; i.e., glasses in this compositional range possess transitional structures.[35] Once the conversion from the modified random network structure to a three-dimensional random network is complete, the properties change again slowly.

Acknowledgment. Work supported by CNR Contract 98.01938.CT03. Authors are grateful to Dr. M. C. Bandini for her performing some of the experiments, to Proff. A. N. Cormack and W. C. LaCourse of the Centre for Glass Research at Alfred University, Alfred, for useful discussion, and to CICAIA (Centro Interdipartimentale Calcolo Automatico e Informatica Applicata, University of Modena and Reggio Emilia) for the Cerius[2] program and other facilities.

References and Notes

(1) Kreidl, N. J. *Glass: Science and Technology*; Academic Press: New York, 1983; p 105.
(2) La Course, W. C. *J. Non-Cryst. Solid* **1976**, *21*, 431 and references therein.
(3) Riebling, E. F. *J. Chem. Phys.* **1996**, *44*, 2857.
(4) Moore, H.; McMIllan, P. W. *J. Soc. Glass Technol.* **1956**, *40*, 97.
(5) Day, D. E.; Rindone, G. E. *J. Am. Ceram. Soc.* **1962**, *45*, 489.
(6) D. E. Day and, G. E. Rindone, *J. Am. Ceram. Soc.* **1962**, *45*, 579.
(7) Taylor, T. D.; Rindone, G. E. *J. Am. Ceram. Soc.* **1970**, *53*, 692.
(8) Lacy, E. D. *Phys. Chem. Glasses* **1963**, *4*, 234.
(9) Osaka, A.; Ono, M.; Takahashi, K. *J. Am. Ceram. Soc.* **1987**, *70*, 242.
(10) McKeown, D. A.; Galeener, F. L.; Brown, G. E. *J. Non-Cryst. Solids* **1984**, *68*, 361.
(11) McKeown, D. A.; Waychunas, G. A.; Brown, G. E. *J. Non-Cryst. Solids* **1985**, *74*, 325.
(12) McKeown, D. A.; Waychunas, G. A.; Brown, G. E. *J. Non-Cryst. Solids* **1985**, *74*, 349.
(13) McKeown, D. A. *Phys. Chem. Glasses* **1987**, *28*, 156.

(14) Greaves, G. N. *J. Non-Cryst. Solids* **1985**, *71*, 203.
(15) Zirl, D. M.; Garofalini, S. H. *J. Am. Ceram. Soc.* **1990**, *73*, 2848.
(16) Cao, Y.; Cormack, A. N. In *Diffusion in Amorphous Materials*; Jain, H., Gupta, D., Eds.; The Mineral, Metals & Material Society: Warrendale, PA, 1994; p 137.
(17) Montorsi, M.; Menziani, M. C.; Leonelli, C.; Pellacani, G. C.; Cormack, A. N. *Mol. Simul.* **2000**, *24*, 157.
(18) Montorsi, M.; Menziani, M. C.; Leonelli, C.; Cormack, A. N. *Mol. Eng*. In press.
(19) Cormack, A. N.; Cao, Y. *Mol. Eng.* **1996**, *6*, 183.
(20) Engelhardt, G.; D. Michel, D. *High-Resolution Solid-state NMR of Silicates and Zeolites*; J. Wiley & Sons: Chichester **1987**.
(21) Maekawa, H.; Maekawa, T.; Kawamura, K.; Yokokawa, T. *J. Phys. Chem.* **1991**, *95*, 6822.
(22) Loewenstein, W. *Am. Mineral.* **1954**, *39*, 92.
(23) Prabkar, S.; Rao, K. J.; Rao, C. N. R. *Eur. J. Solid State Inorg. Chem.* **1992**, *29*, 95.
(24) Schmucker, M.; MacKenzie, K. J. D.; Schneider, H.; Meinhold, R. *J. Non-Cryst. Solids* **1997**, *217*, 99.
(25) Lee, J.; Yano, T.; Shibata, S.; Yamane, M. *J. Non-Cryst. Solids* **1999**, *246*, 83.
(26) Lee, S. K.; Stebbins, J. F. *Am. Mineral.* **1999**, *84*, 937.
(27) Jager, C.; Hartmann, P.; Kunath-Fandrei, G.; Hirsch, O.; Rehak, R. Vogel, J.; Feike, M.; Spiess, H. W.; Herzog, K.; Thomas, B. *Ber. Bunsen-Ges. Phys. Chem.* **1996**, *100*, 1560.
(28) Bradley, S. M.; Hanna, J. V. *J. Am. Chem. Soc.* **1994**, *116*, 7771.
(29) Smith, W.; Forester, T. R. *J. Mol. Graph.* **1996**, *14*, 136.
(30) *Cerius2*; Molecular Simulations, Inc.: San Diego, 1997.
(31) Vessal, B.; Amini, M. Fincham, D.; Catlow, C. R. A. *Philos. Mag. B* **1989**, *60*, 753.
(32) Varshneya, A. K. In *Fundamentals of Inorganic Glasses*; Academic Press: London, UK, 1994; p 146.
(33) Volf, M. B. In *Mathematical Apporach to Glass*; Glass Science and Technology 9; Elsevier: Prague, Czech Republic, 1988; and references therein.
(34) Rao, J. V. Bh. *Phys. Chem. Glasses* **1963**, *4*, 26.
(35) Ray, N. H. IX^e Congrès Internationale Du Verre, Versailles **1971**, *1*, 655.
(36) La Course, W. C.; Cormack, A. N. *Ceram. Trans*. **1998**, *82*, 273.
(37) Dupree, R.; Holland, D.; McMillan, P. W.; Pettifer, R. F. *J. Non-Cryst. Solids* **1984**, *68*, 399.
(38) Engelhardt, G.; Nofz, M.; Forkel, K.; Wihsmann, F. C.; Magi, M.; Samoson, A.; Lippmaa, E. *Phys. Chem. Glasses* **1985**, *26*, 157.
(39) Janes, N.; Oldfield, E.; *J. Am. Chem. Soc*. **1985**, *107*, 6769.
(40) Nofz, M.; Engelhardt, G.; Wihsmann, F. G.; Forkel, K.; Magi, M.; Lippmaa, E. *Z. Chem*. **1986**, *26*, 221.
(41) Murdoch, J. B.; Stebbins, J. F.; Carmichael, I. S: E. *Am. Mineral.* **1985**, *70*, 332.
(42) Grimmer, A.-R.; Magi, M.; Hahnert, M.; Stade, H.; Samoson, A.; Wieker, W.; Lippmaa, E. *Phys. Chem. Glasses* **1984**, *25*, 105.
(43) Klinowski, J.; Ramdas, S.; Thomas, J. M.; Fyfe, C. A.; Hartman, J. S. *J. Chem. Soc., Faraday Trans.* **1982**, *78*, 1025.
(44) Freude, D.; Haase, J.; Klinowski, J.; Carpenter, T. A.; Ronikier, G. *Chem. Phys. Lett.* **1985**, *119*, 365.
(45) Risbud, S.; Kirkpatrick, R. G.; Taglialavore, A.; Montez, B. *J. Am. Ceram. Soc.* **1987**, *70*, C10.
(46) Galant, E. I. *The Structure of Glass*; Consultant Bureau: New York, 1960, 2, p 451.
(47) Stebbins, J. F.; McMillian, P. *J. Non-Cryst. Solids* **1993**, *160*, 116.
(48) Cao, Y.; Cormack, A. N.; Clare, A. G.; Bachra, B. Wright, A. C.; Sinclair, R. N.; Hannon, A. C. *J. Non-Cryst. Solids* **1994**, *177*, 317.
(49) Melman, H.; Garofalini, S. H. *J. Non-Cryst. Solids* **1991**, *134*, 107.